COAL MINING INDUCED LAND SUBSIDENCE MONITORING IN CHINA BY USING TIME SERIES MULTI-FREQUENCY SPACEBORNE INTERFEROMETRIC SAR DATA

PI No. 398

Huanyin Yue[1], Guang Liu[2], Runfeng Wang[3], Xueliang Zhong[4]

[1] National Remote Sensing Center of China, P. R. China
[2] Center for Earth Observation & Digital Earth, Chinese Academy of Sciences, P. R. China
[3] Hebei Bureau of Surveying and mapping, P. R. China
[4] The Institute of Electronics, Chinese Academy of Sciences, P. R. China

1. INTRODUCTION

The coal reserves of china is in the second position among all the countries over the world, china has a big coal output which account for 35% of the whole coal output of the world. Although the coal provide us the energy sources, the coal mining lead a threat to the environment and the life safety of the coal miner. In china coal mining disaster happening every year leads 80% mining caused death all over the world. According to the information provided by the Chinese State Administration of Work Safety, nearly 3000 coal mining disasters happened in 2005, 5491 coal miners died in the disasters, 3639 coal mining disasters happened and 6027 coal miners died in 2004. Although coal mining disasters happen in some national coal mines, many small scales even illegal coal mines are much more liable to be threatened by coal mining disasters because of less equipment for safety and unrestricted mining. Because the mining is underground, it is very hard to supervise the mining beyond the restricted boundary or the illegal mining. It is a big problem for the local government to find and stop the illegal mining to reduce the possibility of mining disasters.

Except for the mining disaster, coal mining induced subsidence is also a threat to the land resources and the safety of buildings. In China, the total area of farmland subsidence induced by coal mining reaches 4000 km^2; 10 thousand tons coal mining lead 2000~6600 m2 land subsidence, the land subsidence area increases 200 km^2 per year. The land subsidence area in Datong coal mine of Liaoning province is 345 km^2, in Jixi coal mine of Heilongjiang province is 156 km^2, in Fuxin coal mine is 109 km^2, in Zibo coal mine is 173 km^2, in Huainan coal mine is 133 km2, in Fengfeng coal mine is 120 km^2, in Tongchuan coal mine of Shanxi is 174 km2, and in Nantong coal mine of Sichuan province is 67 km^2. In Liaoyuan, Jilin province serious subsidence happened with maximum subsidence of 33.3m and rupture of 14.5 m. currently the total loss caused by coal mine subsidence has reaches 50 billion Yuan in China.

Farmers' loss their farmland because of the land subsidence caused by coal mining, which lead serious social problem, and coal mining subsidence damages building and causes landslide in mountainous area as well, the local government is seeking for a method to monitor the mining activity underground. Since monitoring the subsidence is a prerequisite to the relief of damage and possibly a kind of method to monitor the mining activities, people have paid much attention to the subsidence monitoring since the middle of 19 century. The conventional methods like leveling have been applied to the coal mine subsidence monitoring; recently the GPS network is applied to the subsidence monitoring. These methods consist of control point measurements which are discontinuous in both time and space. Aspects involved with this discontinuous knowledge are the availability, representativeness, maintenance and support of stable benchmarks, the survey repeat-rate and duration, the spatial extent and resolution, and the financial restrictions. Improvements in the methodology for coal mine subsidence monitoring, using and combining new instrumentation are necessary to enhance our understanding of subsidence processes and their consequences and decrease financial cost. Differential SAR interferometry (DInSAR) is such technology with a high potential in this aspect.

DInSAR is one promising remote sensing technology for surface subsidence monitoring, which combines synthetic radar imaging theory and electromagnetic wave interferometric technology. Utilizing this technology precise Digital Earth model and millimeter surface subsidence could be achieved theoretically (Massonnet, 1993, Goldstein, 1993, Wright, 2000). DInSAR method can monitor the ground target in continuing time, varied weather condition, and a high spatial resolution about tens of meter scale on very large extend of area, so the cost is relatively lower than conventional methods. DInSAR technique has been applied to the monitoring of mining induced land subsidence in many areas (Urs Wegmuller, et al., 2005; Spreckels V., 2001; Andrew Jarosz and Dieter Wanke, 2004, Herrera, 2007, Ge and et al, 2007).

Because the low coherence areas always exist in many coal mine, recently, the permanent scatterers technique was tried in the mining induced subsidence monitoring in order to overcome the decorrelation phenomena (U. Wegmuller, et al., 2004; Michaela Kircher et al., 2003, Kampes, 2004, George , 2004, Ferretti and et al, 2001, 2007). However, the land subsidence in the coal mine area is very dynamic in time and location with high deformation rate for the long wall mining, the subsidence finished generally within several months; the permanent scatterers technique is not the proper one in such case.

This report is focusing on the feasibility of coal mining area subsidence monitoring by using DInSAR technique, the DInSAR technique is used to process the spaceborne SAR data including C band ENVISAT ASAR and L band JERS SAR and ALOS PALSAR data to derive the temporal land subsidence information from 1993 to 2007 in Fengfeng coal mine area, Hebei province in China, the DInSAR results are compared with leveling data and historical excavation data, the L band shows some advantages in the coal mining induced subsidence monitoring in rural area.

2. DESCRIPTION OF FENGFENG COAL MINE AND DATA

2.1 Fengfeng coal mine

Fengfeng coal mine area locates at the south of Hebei province of China with the size of 560 km2 from 114°3’00’’E to 114°16’40’’E and 36°20’40’’N to 36°34’31’’N, 14 coal mines distribute in this area, the mining depth and coal layer thickness are different in every coal mine, the range of mining depth is from 150m to 1500m, but the mining depth in most coal mines is about 500m, the coal layer thickness is from 1.2m to 6m. The location of Fengfeng coal mine area and the distribution of coal mines are showed in Fig.1.

Fengfeng has 50 years coal mining history, serious land subsidence happened in this area, some subsidence areas has turn to be small lakes, some buildings and constructions were damaged by inhomogeneous deformation. In order to avoid the damage of buildings, recently the coals under buildings are not excavated or some other safety techniques are adopted. Because of the different geological conditions, the magnitude and range of subsidence are different in every coal mines. Generally the subsidence with the magnitude of several dozen centimeters happens in one to three months after the excavation and almost finishes within 3 months; the residual subsidence may last for one year.

2.2 Historical data of coal mining

The historical data of coal mining from 1992 to 2007 was collected; the data include the mining time and position, depth of lane, thickness of coal layer and the ground water condition. In order to make it comparable to the DInSAR results, we collected the mining data between the time of three months earlier than the acquisition date of master image and the date of the slave image for each interferometric pair and draw them into a map.

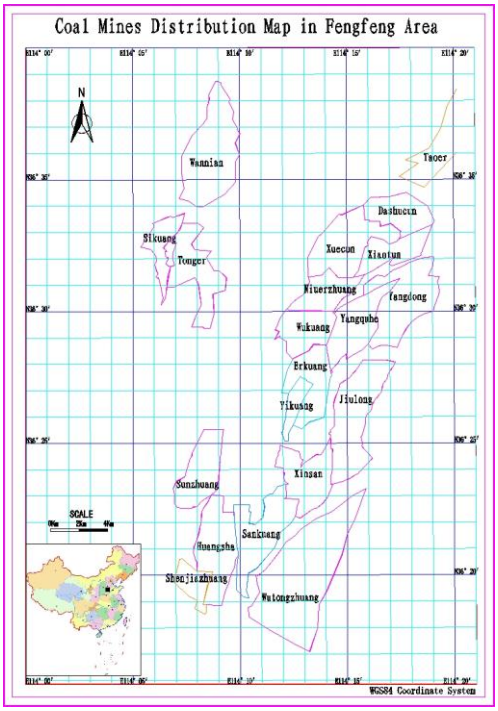

Fig.1 The distribution of coal mines in Fengfeng, Hebei province, China

Fig.2 Distribution of bench marks in Dashucun coal mine and one contour map of land subsidence derived by the leveling data

2.3 Leveling data

In order to test the DInSAR results, optical leveling was undertaken at the same time as the ENVISAT ASAR data acquisition. In Dashucun coal mine, 104 bench marks were installed in an area of 3 km^2, the distribution of these bench marks are shown in Fig.2. The leveling started on April 10th, 2006 and finished on August 5th, 2007 at each time the ENVISAT flies over, so we got 15 leveling data sets, we can derive the subsidence results by the differential values between any two data sets. One of the subsidence contour maps is shown in Fig.2. These subsidence results by leveling

will be compared with the DInSAR results.

2.4 Spaceborne interferometric SAR data

We collected 20 JERS SAR data from 1992 to 1998, 37 ENVISAT ASAR data and 10 ALOS PALSAR data from 2003 to 2008 in Fengfeng area. JERS SAR is an L band sensor with incidence angle of 35 degree and 44 days revisit, but JERS stopped working in 1998. ENVISAT ASAR is a C band sensor with incidence angle of 23 degree and 35 days revisit. ALOS PASLSAR is an L band sensor with incidence angle of 8 to 60 degree and 46 days revisit. Because of the spatial and temporal decorrelation, we only selected the interferometric pairs with small spatial and temporal baseline in the InSAR processing, and then selected 20 interferometric pairs with high coherence to do the differential InSAR processing; all the 20 interferometric pairs are listed on Table.1. These interferometric pairs cover some time intervals from 1993 to 2008, which can reveal the land subsidence evolution in Fengfeng coal mine area.

No.	Sensor	Master orbit	Master acquisition time	Slave orbit	Slave acquisition time	Temporal baseline(days)	Spatial baseline(m)
1	JERS SAR	05722	19930227	06381	19930412	44	1172.9
2		22856	19960416	23515	19950530	44	3474
3		26810	19970105	28787	19970517	132	-251
4		30105	19970813	30764	19970926	44	-1117.2
5		32082	19971223	32741	19980205	44	-1170.5
6		32082	19971223	33400	19980321	44	-1491
7		32082	19971223	34059	19980504	88	634.5
8		32082	19971223	34718	19980617	176	180
9		32741	19980205	33400	19980321	44	-325.4
10		33400	19980321	34059	19980504	44	2120.6
11	ENVISAT ASAR	09333	20031213	09834	20040117	35	560
12		12840	20040814	15345	20050205	175	140.7
13		24542	20061109	25544	20070118	70	-82.5
14		24542	20061109	26546	20070329	140	-119.7
15		25544	20070118	26546	20070329	70	-94.1
16	ALOS PALSAR		20071215		20080130	46	346
17			20081217		20090201	46	524
18			20070730		20070914	46	136
19			20070730		20080501	276	2097

Table.1. Interferometric SAR image pairs used to do the DInSAR processing

2.5 DEM data

The external DEM is SRTM 3 arc second data downloaded from the seamless data distribution system of the Earth Resources Observation and Science of USGS, the data covers the whole processing area in Fengfeng.

3. DIFFERENTIAL INTERFEROMETRIC SAR DATA PROCESSING AND RESULTS

The phase of SAR interferogram includes reference phase, topographic phase, deformation phase, atmospheric phase and noise. If the deformation velocity is high, then the atmospheric phase and noise could be ignored. After removal of the reference phase and the topographic phase, the deformation phase could be directly obtained. The quality of the interferometric phase is related with thermal noise, temporal baseline, image miscoregistration, spatial baseline and etc.., the quantified description of the quality is coherence or correlation (Howard, 1992, Srivastava, 2006). In common situation, the thermal noise will be controlled to a low level with deliberated design of the sensor system, and the larger the temporal baseline and spatial baseline, the less precision of the image coregistration, the lower of the coherence, which means the quality decrease of the interferograms. In this study, the open source software DORIS from TU-Delft is used. For ASAR data processing, the precise orbits from ESA or from TU-Delft could be used, the accuracy is about 5 cm radial and about 15 cm in along and cross-track direction, so based on the precise orbit, the reference phase and topographic phase could be easily removed. For JERS1 data, there is no precise orbit information provided by JAXA, and the orbit information in ephemeris come from SLR measurements, the accuracy is about tens of centimeters, a precise orbit re-estimation method should be developed to avoid errors when using the ephemeris data in DInSAR processing. For PALSAR data, since ALOS has a GPS instrument on board, the orbit error is smaller than JERS1, but since the ephemeris time gap is one minute, the orbit interpolation method will cause errors during DInSAR Processing.

3.1 Baseline Re-estimation

Spatial baseline is an important factor in SAR interferometry, JERS has no GPS on board, baseline re-

estimation is needed for DInSAR processing, or otherwise the orbit error will propagate into the phase of interferogram and cause wrong result. Nowadays, most of the baseline re-estimation methods are based on linear baseline error model. This might not be accurate enough, since all the software now using a high degree polynomial or spline function to model satellite orbit, theoretically it will be reasonable to model the baseline error as high polynomial or spline function.

In this study, a dynamical coordinate system called *RXA* is setup, where R is a vector directing from the target to the corresponding position on the orbit, A is the vector of satellite velocity, X is normal to both R and A to construct a right hand coordinate system (Liu Guang, 2007). Generally the spatial baseline error can be described as:

$$\delta\vec{B}_l = (a_0 + a_1 l + a_2 l^2 + \cdots + a_n l^n)\vec{B}_\perp + (b_0 + b_1 l)\vec{B}_{//}$$

A high degree polynomial is use to model the baseline error, where the first part of this equation is perpendicular baseline error:

$$\delta B^l{}_\perp = (a_0 + a_1 l + a_2 l^2 + \cdots + a_n l^n)$$

The second part of this equation is parallel baseline error:

$$\delta B^l{}_{//} = b_0 + b_1 l$$

And l is the line number of the SAR image. Since the existed coupling between perpendicular baseline error and parallel baseline error, a "two steps" method is used to decoupling the baseline error. In perpendicular baseline rectification, we select some lines $(l_0, l_1, \cdots, l_m)$ randomly in the interferogram and estimate the phase frequency by Fourier Transformation so as to calculate the perpendicular baseline error on lines, and then use Eq.2 to estimate $(a_0, a_1, \cdots, a_n)$. Doing similar processing in the azimuth direction allows estimating parallel baseline error, and the parameters (b_0, b_1) could be obtained. In this processing, the singular value of phase frequency was removed by the ***DIA*** method (P.J.G. Teunissen, 2000).

3.2 DEM Autocoregistration to SAR image

In order to get the information of surface subsidence, the topography phase has to be removed. In this study "two pass" method is used, it use an external DEM and sensor orbits, in virtue of the SAR imaging geometrical relationship to simulate the topographic phase. This method is quite straight, and it is usually preferred. Still there is a problem of the phase simulated method, because of the positional errors and geometrical distortion of external DEM, the simulated phase image then may have a small shift to SAR image, this always cause wrong phase information for monitoring subsidence.

Here we present a method to reduce the positional error of external DEM in phase simulation method (Liu Guang, 2009). First the intensity SAR image is simulated. There are two factors affecting the SAR image intensity, one is the surface characteristic, the other is the local incidence angle, the relationship could be expressed as equation (D.O. Muhleman, 1964):

$$Intensity = D_{const}\frac{\cos I}{(\sin I + 0.1\cos I)^3}$$

I is the local incidence angle, in common situation, the local incidence angle have dominant effect when SAR is imaging the ground target. Local incidence angle is related to the incidence angle and surface normal, when local incidence angle equal to zero, we will get the strongest backscattering, when the angle is large than 90°(positive in clockwise direction), there will be shadows, and if angle is small than 90°, layover will happen. In SAR intensity image simulation, the key point is to find out the incidence angle for every pixel on the SAR image. So, now the question is simplified, and the solution is simple. First for every point on the external DEM, the position $(l, p)_{DEM}$ on the master image coordination system could be computed, the number of $(l, p)_{DEM}$ is always not an integer, then for every grid position $(l, p)_{SAR}$ on SAR image, we can find three nearest points $(l, p)_{DEM}$, we say $(l, p)^A{}_{DEM}$, $(l, p)^B{}_{DEM}$, $(l, p)^C{}_{DEM}$, this is a 3D space triangle, and all these three points have their own 3D coordination, using a simple relationship for triangle we can compute the surface Normal:

$$\hat{n} = [(l, p)^A{}_{DEM} - (l, p)^B{}_{DEM}] \times [(l, p)^A{}_{DEM} - (l, p)^C{}_{DEM}]$$

For incidence angle, there is a trick. We are not computing this angle directly, but the incidence vector is computed using SAR image geometry, and the local incidence angle is computed as an inner product of Surface Normal and Incidence vector. After get the simulated SAR intensity image, we can compute the coregistration polynomial for the simulated intensity image and SAR image, using the same coregistration polynomial, the simulated phase image can be resampled into a correct position, and then be removed.

4. RESULTS AND ANALYSIS

4.1 DInSAR results

The area we cropped locates at the east of Fengfeng coal mine area, covering 8 coal mines, the center coordinates is 114.25□E, 36.25□N with a size of 25km in the azimuth and 15 km in the range. Fig 3 shows the 17 differential interferometric results which have been filtered to reduce the noise. The land subsidence results derived from JERS data are shown in Fig 3a to Fig 3j, the results derived from ASAR data are shown in Fig 3k to Fig 3o, and the results derived from ALOS PALSAR data are shown in Fig.3p to Fig.3s. In all these interferograms, the spatial baseline is smaller than 1172 meters in L band and 140.7 meters in C band, the temporal baseline is smaller than 176 days in L band and 175 days in C band. Normally, interferometric pairs with small spatial baselines in the same season have higher coherence.

Because most area in Fengfeng are covered by crops or grass from spring to autumn, L band radar signal can penetrate the vegetation much easier than C band, and L

band is less affected by the atmosphere than C band, generally the JERS data and ALOS PALSAR data have higher coherence than ASAR data in these 17 interferograms. Because of the changes of crops and grass on the surface in different seasons, most interferometric pairs of JERS and ALOS PALSAR with higher coherence are in the same season. It is very hard to get deformation results by the ASAR data in different seasons, all the deformation results of ASAR data except for Fig 3i are in winter without the influence of crops and grass. The villages have good coherence but generally no deformation happened there, because no excavation was undertaken under such places.

Although the L band interferometry can keep higher coherence, the C band interferometry is more sensitive to the surface deformation; it can detect deformation with smaller magnitude. For 3 centimeters deformation, it reveals 1/4 fringes on L band interferogram, whereas more than one fringe on C band interferogram. Generally the deformation decreases from the highest value to zero when it goes from the subsidence center to the edge, so the C band interferometry can detect a bigger range of subsidence with more fringes, but with lower coherence than the L band.

Fig.3 showed a history of the underground mining activities, JERS is an earlier launched SAR satellite, we could got the "snapshots" of the surface deformation in different periods during year 1993 to 1998, and ENVISAT is launched in 2002, so we could got the deformation information after 2002, and ALOS was on orbit since 2006, so the interferogram will reflect the surface movement after 2006. Actually, by multi-band D-InSAR we can obtain relatively long history information of deformation and thus give a comprehensive understand of the situation of the underground activities.

4.2 Levelling results and DInSAR results

In the experiment, the leveling in Datun coal mine was designed to be undertaken at the SAR image acquisition time of Frame2871, Track261 of ENVISAT, but there is no good differential interferometric results derived from the data set of Frame2871, Track261, all the effective differential interferometric results are derived from the data set of Frme729, Track440, so there is a delay between the time of leveling and the SAR image acquisition.

We overlaid the leveling contour maps and the differential InSAR results, which are showed in Fig 4a-Fig 4c, the black lines on the maps is the boundary of the coal mines. From all the maps of Fig 4, we can see the subsidence positions on the leveling contour maps and the differential fringes are consistent with each other. We also compared the subsidence magnitude of both leveling and DInSAR results. Because the DInSAR result can only reflect the deformation of LOS direction, in order to be comparable with the leveling data, we derived the vertical deformation from the LOS component divided by cos23□. The maximum subsidence values on DInSAR fringe maps are about 330, 190, 270 millimeters respectively on Fig.4a, Fig.4b and Fig.4c. Comparing these DInSAR results with the maximum value measured by leveling, we can see they are also consistent with each other. From this experiment, it shows the subsidence position and magnitude in all coal mines detected by the DInSAR technique are reliable.

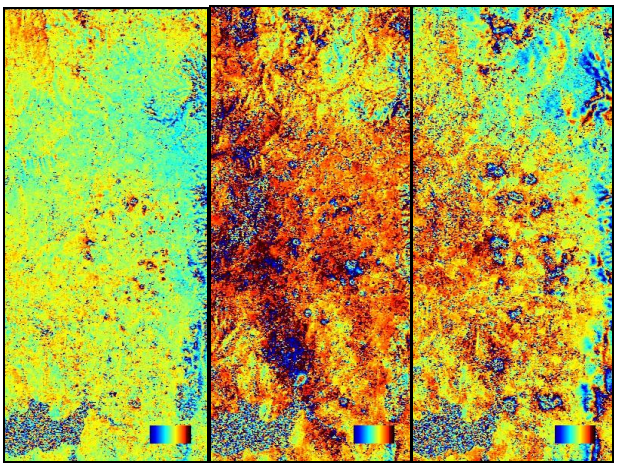

a.199302-199304 b.199604-199605 c.199701-199705

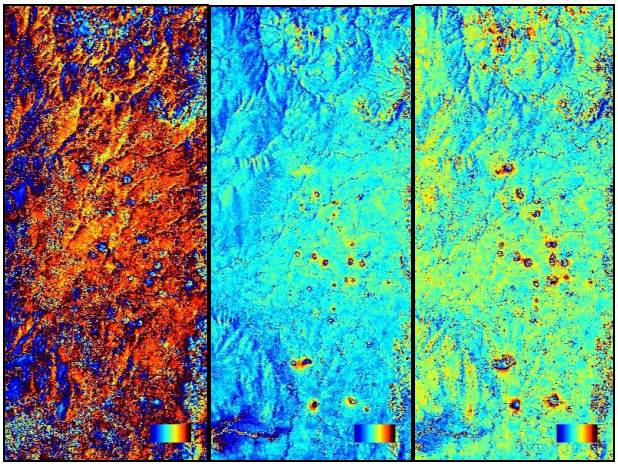

d. 199708-199709 e. 199712-199802 f. 199712-199803

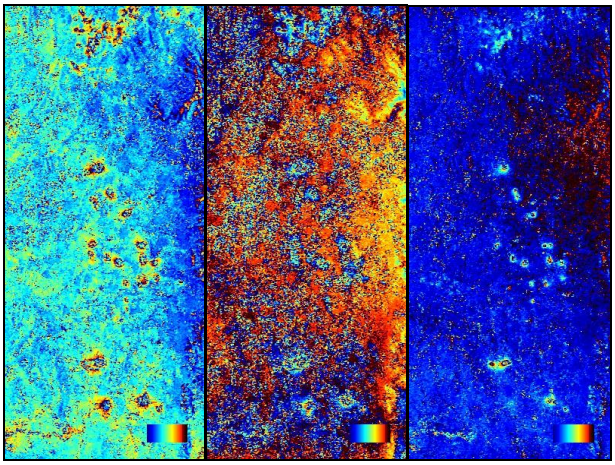

g. 199712-199805 h. 199712-199806 i. 199802-199803

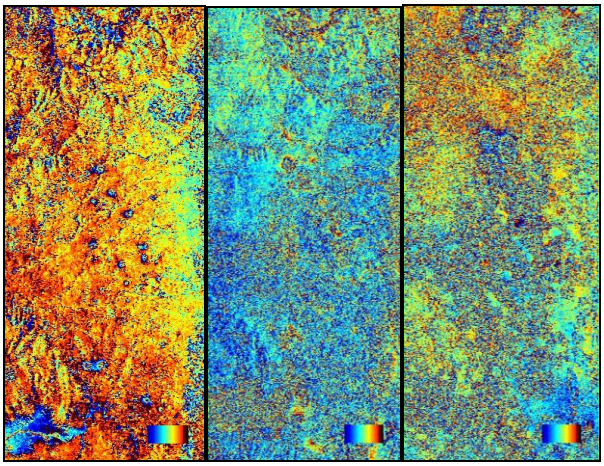

j. 199803-199805 k. 200312-200401 l. 200408-200502

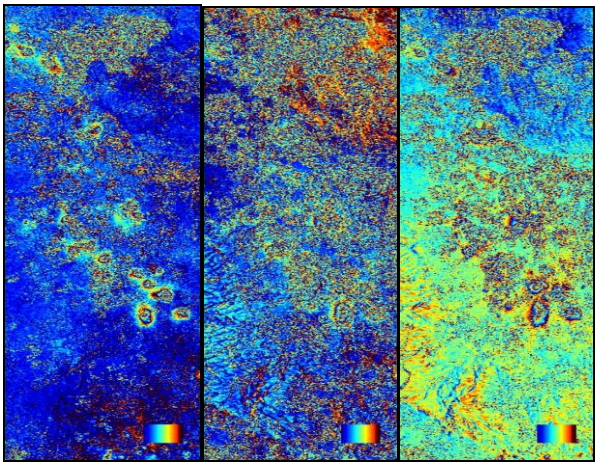

m. 200611-200701 n. 200701-200702 o. 200701-200703

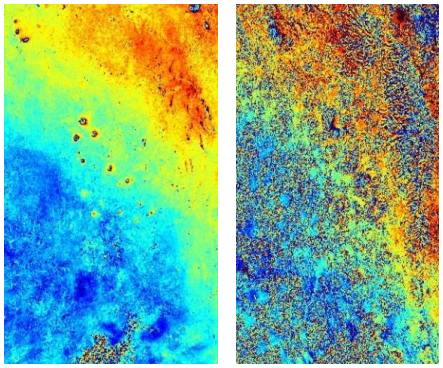

p. 200707-200709 q.200707-200805

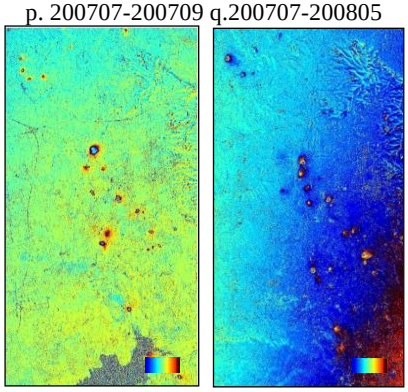

r. 200712-200801 s. 200812-200902

Fig.3. Land subsidence results derived by DInSAR in different time intervals. Fig. 3a-3j were derived by JERS data, fig. 3k-3o were derived by ASAR data, fig. 3p-3s were derived by ALOS PALSAR data. JERS data and ALOS PALSAR data have higher coherence than ASAR data in these results.

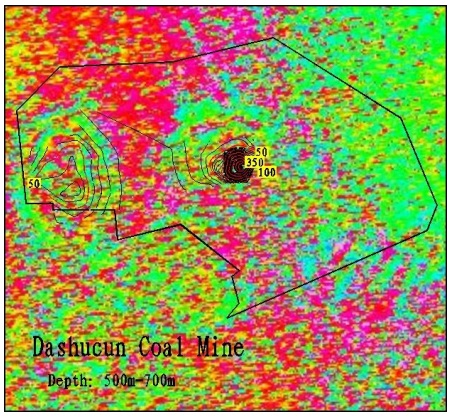

a. DInSAR time: 2006/10/5-2007/2/22
Leveling time: 2006/10/28-2007/02/01

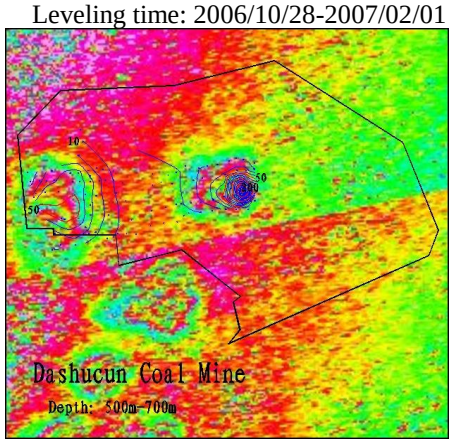

b. DInSAR time: 2006/11/9-2007/01/18
Leveling time: 2006/10/28-2007/01/08

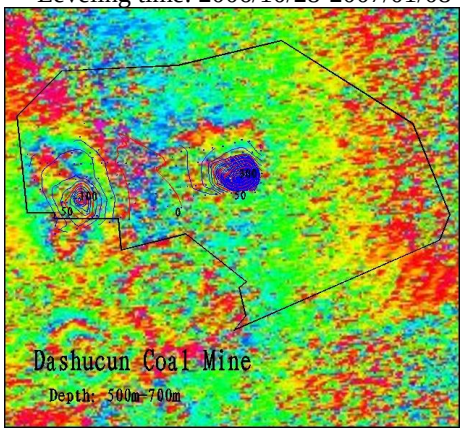

c. DInSAR time: 2007/01/18-2007/03/29
Leveling time: 2007/01/08-2007/03/10

Fig.4. Comparison between the DInSAR result and leveling result in Dashucun coal mine. The unit of the values of leveling data is milimeter

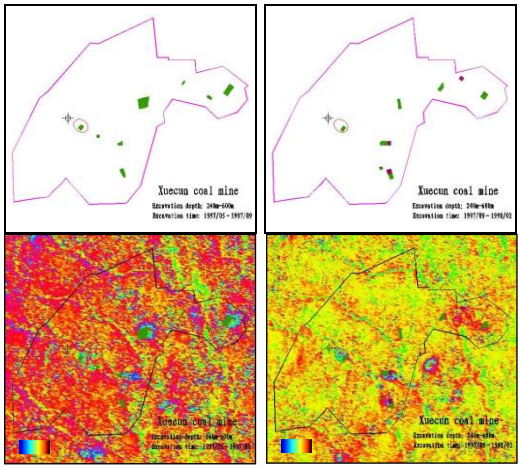

a. 1997/08~1997/09 b. 1997/12~1998/02

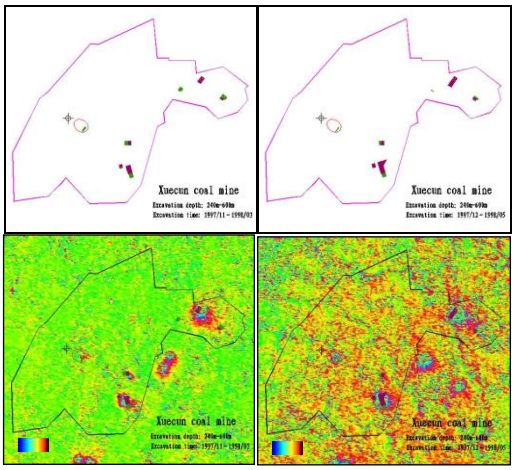

c. 1998/02/05~1998/03/21 d. 1998/03~1998/05

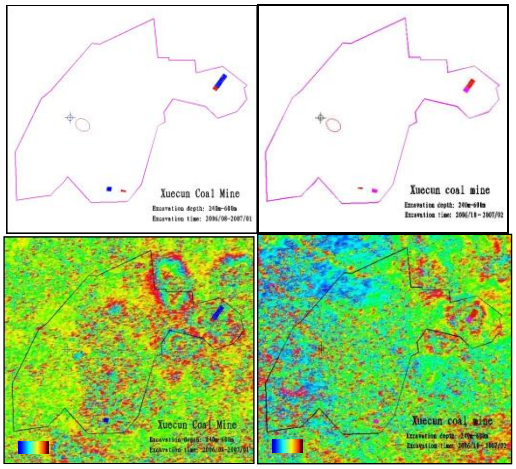

e. 2006/11~2007/01 f. 2007/01~2007/02

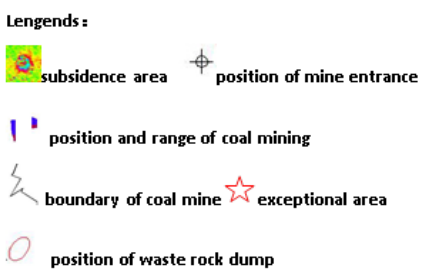

Fig.5. Comparison between DInSAR land subsidence results of ASAR and historical excavation data in Xuecun coal mine

4.3 DInSAR results and historical coal mining data

After we validate the reliability of the DInSAR results, we overlaid each geo-coded interferogram with the historical excavation data. The interferogram covers 8 coal mines in Fengfeng area, it is difficult to analyze all the coal mines in one paper, we only select Xuecun coal mine as our test site. Fig 5 shows the temporal changes of the range and position of land subsidence and the mining location. In Fig 5, there are totally 35 mining locations in the different time intervals, and 28 subsidence areas on the mining location are detected obviously by the DInSAR technique, the detection precision is higher than 80%. But there are still 7 mining locations which are not detected by the DInSAR technique, the subsidence at these locations might have finished at the time interval we detected by DInSAR, or the residual subsidence might be very small, most likely the InSAR signal is affected by the decorrelation noise caused by the ground changes and the spatial baseline, or the weak deformation signal is contaminated by the atmospheric artifacts.

4.4 Possibility of coal mining activities monitoring by DInSAR data

In the above contents we show the DInSAR technique is feasible to monitor the coal mining induced land subsidence, the position of DInSAR land subsidence is coincidence with the position of underground excavation. In order to see whether the DInSAR technique can monitor the mining activities, we need further analysis.
We need to know the land subsidence difference between the interferograms before and after coal mining activity. Fig 6 shows one example of surface changes above the local mining lanes. From Fig 6 we can see there is no subsidence before the excavation, however, when the mining happens, the DInSAR can detect the subsidence induced by coal mining, so the coal mining position and time can be detected by the DInSAR, although there is several months delay.

CONCLUSION

Spaceborne DInSAR technique can be used to derive the feasible land subsidence map in coal mines, which is useful information in monitoring the underground coal mining activities from space. However high coherence of the interferometric pair is necessary in such application, a small spatial baseline and a small temporal baseline in the same season are required especially in the rural area. Compared with L band SAR such as PALSAR and JERS, C band SAR need much smaller spatial and temporal baseline and the subsidence center will always lose

information because of decorrelation, but it is obviously more sensitive to the deformation. So, C band is suitable for low velocity subsidence with short temporal baseline, while L band will have advantage for longer time span. Although the accuracy of subsidence detection of L band is lower than C band, L band SAR interferometry can keep higher coherence, time series L band SAR data can form more effective differential InSAR results.

ACKNOWLEDGEMENT

Thanks ESA CAT-1 project no.4288 and JAXA ALOS RA2 project.

REFERENCE

[1] Ferretti, G. Savio, R. Barzaghi, A. Borghi, S. Musazzi, F. Novali, C. Prati, F. Rocca, “Submillimeter accuracy of InSAR time series: experimental validation”, IEEE Transactions on Geoscience and Remote Sensing. 45 (5), 1142–1153, 2007.

[2] Jarosz and D. Wanke, "Use of InSAR for monitoring of mining deformation", Proc. of FRINGE 2003 Workshop, Frascati, Italy, 1-5 December, 2003.

[3] Bert M Kampes. Displacement Parameter Estimation using Permanent Scatterer Interferometry. PhD thesis, DLR, 2004. Kluwer Academic Publishers.

[4] D.O. Muhleman, "Radar scattering from Venus and Moon", Astronomic Journal, 24, pp.34-40, 1964.

[5] Didier Massonnet and Thierry Rabaute. Radar interferometry: Limits and potential. In IEEE Transactions on Geoscience and Remote Sensing, pages 455–464, 1993.

[6] Ferretti, A., Prati, C., & Rocca, F.. Permanent Scatters in SAR Interferometry. IEEE Transactions on Geosciences and Remote Sensing, 39, 8−20, 2001.

[7] G. Herrera, R. Toms, J.M. Lopez-Sanchez, J. Delgado, J.J. Mallorqui, S. Duque, and J. Mulas, “Advanced DInSAR analysis on mining area : La Union case study (Murcia, SE Sapin)”, Engineering Geology, 90, 148−159 p, 2007.

[8] G. Liu, "Mining area subsidence monitoring using Multi-band SAR data", 2009 Urban Remote Sensing Joint Event, 20-22 May, 2009, ShangHai, P. R. China

[9] G. Liu, "Research on orbits adjustment and image coregistration in time series radar interferometry", PhD Thesis, 2007, Institute of Remote Sensing Applications Chinese Academy of Sciences, P.R. China

[10] George E Hilley, Roland Burgmann, Alessandro Ferretti, Fabrizio Novali, and Fabio Rocca. Dynamics of slow-moving landslides from Permanent Scatterer analysis. Science, 304:1952–1955, June-25 2004.

[11] Howard A Zebker and John Villasenor. Decorrelation in interferometric radar echoes. IEEE Transactions on Geoscience and Remote Sensing, 30(5):950–959, September 1992.

[12] Linlin Ge, Hsing-Chung Chang, and Chris Rizos, “Mine Subsidence Monitoring Using Multi-source Satellite SAR Images”, Photogrammetric Engineering & Remote Sensing, Vol. 73, No. 3, March 2007, pp. 259–266.

[13] M. Kircher, J. Hoffmann, A. Roth, B. Kampes, N. Adam and H. J. Neugebauer, "Application of permanent scatterers on mining-induced subsidence", Proc. of FRINGE 2003 Workshop, Frascati, Italy, 1-5 December, 2003.

[14] P.J.G. Teunissen, "Adjustment theory: an introduction", Delft University Press, Delft, 1 edition, 2000.

[15] R M Goldstein, H Engelhardt, B Kamp, and R M Frolich. Satellite radar interferometry for monitoring ice sheet motion: Application to an Antarctic ice stream. Science, 262:1525–1530, 1993.

[16] Srivastava, H.S., Patel, P. and Navalgund, R.R., Application potentials of synthetic aperture radar interferometry for land-cover mapping and crop-height estimation. Current science, 91(6), pp. 783-788, 2006.

[17] Tim J Wright. Remote monitoring of the earthquake cycle using satellite radar interferometry. Phil. Trans. R. Soc. Lond. A, 360:2873–2888, 2002.

[18] U. Wegmuller, C. Werner, L. Petrat, T. Strozzi, A.Wiesmann, and N. Benecke, "EOMD mining project-improvements to the EO service part", ENVISAT-ERS Symposium, Salzburg 2004.

[19] U. Wegmuller, V. Spreckels, C. Werner, T. Strozzi and A. "Wiesmann, Monitoring of mining induced surface deformation using L-band SAR interferometry", Int. Geosci. Rem. Sens. Symp. 2, 1232-1235 (2005).

[20] V. Spreckels, J. Musiedlak, U. Wegmuller, T. Strozzi, and C. Wichlacz, "Detection of underground coal mining-induced surface deformation by differential InSAR data", ISPRS WG I/2,I/5,IV/7 Workshop on Hign resolution mapping from space, Hannover, Germany, 19-21 September 2001.